

Article

Broadband Generalized Sidelobe Canceler Beamforming Applied to Ultrasonic Imaging

Jiake Li ^{1,*} , Zhe Ma ¹, Lei Mao ¹, Zhengjun Wang ², Yi Wang ³ , Huaiyu Cai ³ and Xiaodong Chen ^{3,*}

¹ X LAB, The Second Academy of CASIC, Beijing 100854, China; mazhe_thu@163.com (Z.M.); 13910138990@139.com (L.M.)

² Beijing Mechanical Equipment Institute, Beijing 100854, China; wzj_greensir@163.com

³ School of Precision Instrument & Opto-electronics Engineering, Tianjin University, Key Laboratory of Optoelectronics Information Technology (Tianjin University), Ministry of Education, Tianjin 300072, China; koala_wy@tju.edu.cn (Y.W.); hycail@tju.edu.cn (H.C.)

* Correspondence: lijake1223@163.com (J.L.); xdchen@tju.edu.cn (X.C.)

Received: 23 November 2019; Accepted: 6 February 2020; Published: 11 February 2020



Abstract: A broadband generalized sidelobe canceler (Broadband-GSC) application for near-field beamforming is proposed. This approach is implemented in the wavelet domain. Broadband-GSC provides a set of complex, adapted apodization weights for each wavelet subband. The proposed method constrains interference and noise signal to improve the lateral resolution with only one single emission. Performance of the proposed beamforming is tested on simulated data obtained with Field II. Experiments have proved that the new beamforming can significantly increase the image quality compared with delay-and-sum (DAS) and synthetic aperture (SA). Imaging of scattering points show that Broadband-GSC improves the lateral resolution by 43.2% and 58.0% compared with SA and DAS, respectively. Meanwhile, Broadband-GSC reduces the peak sidelobe level by 11.6 dB and 26.4 dB compared with SA and DAS, respectively. Plane wave emission experiment indicates that Broadband-GSC can improve the lateral resolution by 44.2% compared with DAS. Furthermore, the new beamforming introduces the possibility for higher frame-rate and higher investigation depth with increased lateral resolution.

Keywords: adaptive beamforming; wavelet; phased array; lateral resolution

1. Introduction

Ultrasonic imaging with characteristics of high transmission capacity and low harm to the human body has become one of the major medical diagnostic technologies nowadays. Imaging algorithms are the key technology of ultrasonic imaging system [1], while delay-and-sum (DAS) is one of the most widely used non-adaptive beamforming methods. However, DAS suffers from low lateral resolution and low signal-noise-ratio (SNR) [2]. In order to improve the imaging quality of the ultrasonic system, different kinds of adaptive beamformings have been introduced to process the ultrasonic echo data [3–7]. The calculated data-dependent apodization weights are equivalent to a spatial filter, which can maintain the desired signal and suppress the interference and noise signal of the ultrasonic echo data.

Almost all previous work within this field is characterized by the fact that narrowband methods have been directly applied on broadband ultrasonic echo data [8,9]. Therefore, Jørgen Arendt Jensen proposed a broadband minimum variance beamforming implemented in the frequency domain [10,11]. Jørgen Arendt Jensen introduces the sub-discrete Fourier transform (sub-DFT) to divide the broadband echo signal into a set of narrowband signals, and provides a set of adapted, weights for each frequency

subband. However, how to appropriately divide the broadband signal into a set of narrowband signals based on sub-DFT needs more exploration. Appropriate division determines the quality of the system, thus sub-DFT beamforming is faced with the problem of decreased robustness [12,13].

This paper proposes an approach implemented in the wavelet domain. First, broadband echo signals are divided into a set of narrowband signals with discrete wavelet transform. Then, each wavelet subband is processed independently by a narrowband beamforming, generalized sidelobe canceler. Later, the processed subband responses are coalesced to provide the broadband beamforming output.

The outline of this paper is as follows: Section 2 focuses on the traditional methodologies and its application to ultrasonic imaging. Section 3 looks into the principle and realization of the broadband generalized sidelobe canceler in detail. Section 4 presents the experiment results based on simulated data. Finally, the advantages of the proposed beamforming and its comparison with early proposed methodologies are discussed and concluded in Section 5.

2. Background

The diagram of the traditional ultrasonic imaging beamforming method is shown in Figure 1. First, one single element is excited to transmit the ultrasonic, and all elements receive the echo signal. Delay-and-sum (DAS) is introduced to obtain a receiving focused echo image, with low lateral resolution [14]. Then, exciting each element in turn, N's receiving focused images will be achieved. Later, N's receiving focused images are summed together to form the final beamforming output. Synthetic aperture (SA) is a passive process using fixed, data-independent apodization weights. The phase-shift can be implemented as time-delay and space-delay, therefore, SA achieves both receiving and transmitting focused [15,16]. The non-adaptive beamforming DAS and SA works for both narrowband and broadband signals.

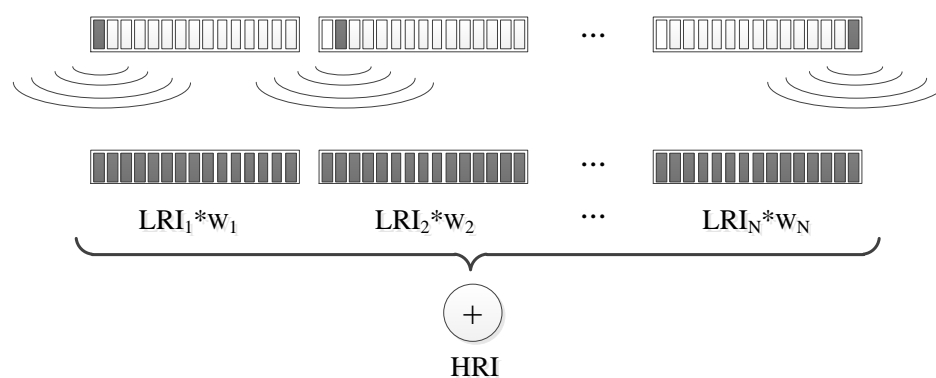


Figure 1. The diagram of synthetic aperture.

For narrowband signals, adaptive beamforming is simply an extension of the SA. The only difference is the choice of apodization weights. Instead of using predefined, data-independent apodization weights, the adaptive beamforming actively updates a set of new weights that are dependent on the received echo data.

2.1. Non-Adaptive Beamforming

Delay-and-sum (DAS) is adopted to obtain the receiving focused echo signal. The sensor elements' response from the focus point will be added up in phase. Consequently, the desired signal from the focus point will be maximized. An arbitrary point $\forall \vec{r}_p = (x, z)$ is carried out by compensating for the propagation delay profile for this point. The delay is calculated as the propagation path from the nth

transmitting element to the focus point and back to the mth receiving element. For a phased transducer array of M elements, the propagation path is given by:

$$k_{nm}(\vec{r}_p) = \frac{\|r_n^{\vec{x}mt} - \vec{r}_p\| + \|r_m^{\vec{r}cv} - \vec{r}_p\|}{c} \times fs \tag{1}$$

where n and m represent the transmitting and receiving element, respectively. N and M represent the number of elements of the transmitting and receiving array, which are usually equal to total element number of the array, respectively. $n = 1, 2, \dots, N$; $m = 1, 2, \dots, M$. $r_n^{\vec{x}mt}$ and $r_m^{\vec{r}cv}$ are spatial positions of the transmitting element and the receiving element, respectively. c is the ultrasonic velocity, fs is the sampling rate of ultrasonic system. The receiving focused echo image with low lateral resolution (LRI, low-resolution imaging) is given by:

$$LRI_n = \sum_{m=1}^M \omega_m \times x_{nm}(k_{nm}(\vec{r}_p)) \tag{2}$$

As all elements are excited in turn, N's LRI echo imaging will be obtained. Overlay all these LRIs with predefined, data-independent apodization weights, echo image with both transmitting and receiving focused is obtained. The newly achieved ultrasonic imaging is the response after synthetic aperture (SA), also known as the high-resolution imaging (HRI).

$$HRI = \sum_{n=1}^N \omega_n \times LRI_n \tag{3}$$

2.2. Generalized Sidelobe Canceler

Generalized sidelobe canceler (GSC) belongs to adaptive beamforming, which can be expressed as the following constraint conditions. GSC can maintain the desired signal and suppress the interference and noise signal.

$$\min \omega^H \mathbf{R} \omega, \text{ subject to } \omega^H \mathbf{a} = 1 \tag{4}$$

where **a** is the steering vector, which represents the direction of desired signal. For both transmitting and receiving the focused echo signal, **a** is a unit vector. **R** is the interference and noise covariance matrix. The superscript $\{\cdot\}^H$ denotes the conjugate transpose. Adaptive beamforming GSC separates the linear constraints with an adaptive filter. Therefore, the constrained optimization problem of formula (4) is converted into an unconstrained optimization problem. The apodization weights after GSC can be expressed as [17]:

$$\omega = \omega_q - \mathbf{B} \omega_a \tag{5}$$

ω_q and ω_a are temporal non-adaptive weight vector and adaptive weight vector, respectively. ω_q is determined by received echo signals, $\omega_q = (\mathbf{a} \mathbf{a}^H)^{-1} \mathbf{a}$. ω_a is determined by the interference and noise signal, $\omega_a = (\mathbf{B}^H \mathbf{R} \mathbf{B})^{-1} \mathbf{B}^H \omega_q$. **B** is a $N * (N - 1)$ dimensional blocking matrix, which can block off the desire signal with the interference and noise signal [18]. The blocking matrix **B** must satisfy $\mathbf{B}^H \mathbf{a} = 0$.

The weight vector can be calculated when the interference and noise covariance matrix **R** is obtained. In practical application, **R** is replaced by the sample covariance matrix $\hat{\mathbf{R}}$:

$$\hat{\mathbf{R}} = \frac{1}{2K + 1} \sum_{k=-K}^K \mathbf{x}(k) \mathbf{x}(k)^H \tag{6}$$

where $2K + 1$ represents the number of echo signal used to construct the $\hat{\mathbf{R}}$. $\mathbf{X}(k) = [\mathbf{LRI}_1(k), \mathbf{LRI}_2(k), \dots, \mathbf{LRI}_N(k)]^T$, which means the time-delayed echo signal. The final echo imaging after GSC can be expressed as:

$$\mathbf{y}(k) = \boldsymbol{\omega}^H(k)\mathbf{X}(k) \tag{7}$$

3. Proposed Method

The adaptive beamforming GSC [19] was originally proposed for narrowband applications. The ultrasonic echo data is the broadband signal [20]. Therefore, the broadband ultrasonic echo signals need be divided into a set of narrowband signals [21]. The discrete wavelet transform is introduced to divide the ultrasonic echo signals. Each separated subband fulfills the narrowband condition, and each separated subband is processed independently.

For narrowband echo signals, the adaptive beamforming is an extension to the DAS. As illustrated in Figure 2, firstly, proposed beamforming uses the discrete wavelet transform (DWT) to divide the broadband echo signal into a set of narrowband signals. Then, the sets of narrowband signals after DAS are fed to the adaptive processor GSC, consequently, provides a set of adapted apodization weights for each wavelet subband. Later, beamformed narrowband ultrasonic echo signals are coalesced. Finally, the inverse discrete wavelet transform (IDWT) is adopted to deal with the coalesced broadband echo signals, and the broadband echo imaging will be achieved.

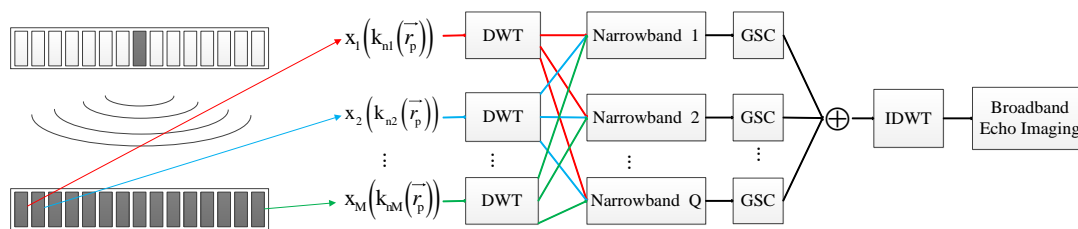


Figure 2. The block diagram of broadband generalized sidelobe canceler.

For the given focus point $\forall \vec{r}_p = (x, z)$, the beamforming output for each wavelet subband, $\text{NB}_q(\vec{r}_p)$, is given by:

$$\text{NB}_q(\vec{r}_p) = \sum_{m=1}^M \omega'_m(\omega_q) Y_m(\omega_q) \tag{8}$$

$Y_m(\omega_q)$ is the discrete wavelet transform response of the m th element's echo signal at q th wavelet subband. $\omega_m(\omega_q)$ is the adapted apodization weight for the q th wavelet subband, which is obtained with adaptive beamforming GSC. $\{\cdot\}'$ denotes the complex conjugate. For each wavelet subband, defining the apodization weight vectors and the wavelet subband response vectors:

$$\boldsymbol{\omega}(\omega_q) = [\omega_1(\omega_q), \omega_2(\omega_q), \dots, \omega_M(\omega_q)]^T \tag{9}$$

$$\mathbf{Y}(\omega_q) = [Y_1(\omega_q), Y_2(\omega_q), \dots, Y_M(\omega_q)]^T \tag{10}$$

Superscripts $\{\cdot\}^T$ denote the non-conjugate transpose. The beamforming output for each wavelet subband can be rewritten as:

$$\text{NB}_q(\vec{r}_p) = \boldsymbol{\omega}^H(\omega_q)\mathbf{Y}(\omega_q) \tag{11}$$

Using the inverse discrete wavelet transform to deal with the coalesced broadband echo signals $\mathbf{NB}(\vec{r}_p) = [\text{NB}_1(\vec{r}_p), \text{NB}_2(\vec{r}_p), \dots, \text{NB}_Q(\vec{r}_p)]$. Q represents the total number of the wavelet subband. The final broadband echo imaging (Bi) will be achieved using inverse discrete wavelet transform (IDWT).

$$\text{Bi} = \text{IDWT}(\mathbf{NB}(\vec{r}_p)) \tag{12}$$

4. Results

In this section, several examples are provided to compare performance of the proposed beamforming with DAS, SA, and GSC in terms of lateral resolution, sidelobe level and contrast. A simulation tool named Field II is used to calculate the simulated ultrasonic echo data, which is highly accepted in the medical ultrasonic imaging field [22,23]. Simulated echo data can be used to verify the beamforming performance of the algorithm. Field II is used to obtain the simulated echo signal of scattering points and the circular cyst of a linear phased array ultrasonic system. Key parameters of the simulated linear phased array ultrasonic system are listed here: width of array $d = 0.2413$ mm; center frequency of the ultrasonic $f_0 = 3.33$ MHz; array number $M = 64$; ultrasonic velocity $c = 1500$ m/s; sampling rate of system $f_s = 71.04$ MHz.

4.1. Simulated Point Targets

Fourteen scattering points are set up in the imaging area. Figure 3 shows the beamforming responses. Beamforming responses of the DAS are the results after delay-and-sum, which the 32nd element generates ultrasonic and all elements receive echo signal [24]. Figure 4 shows the lateral variation of the beamforming responses at two different depths, $z = 41$ mm and 45.8 mm, respectively. Figure 4 indicates the peak sidelobe level (PSL) and the full width at half maximum (FWHM) after each beamforming.

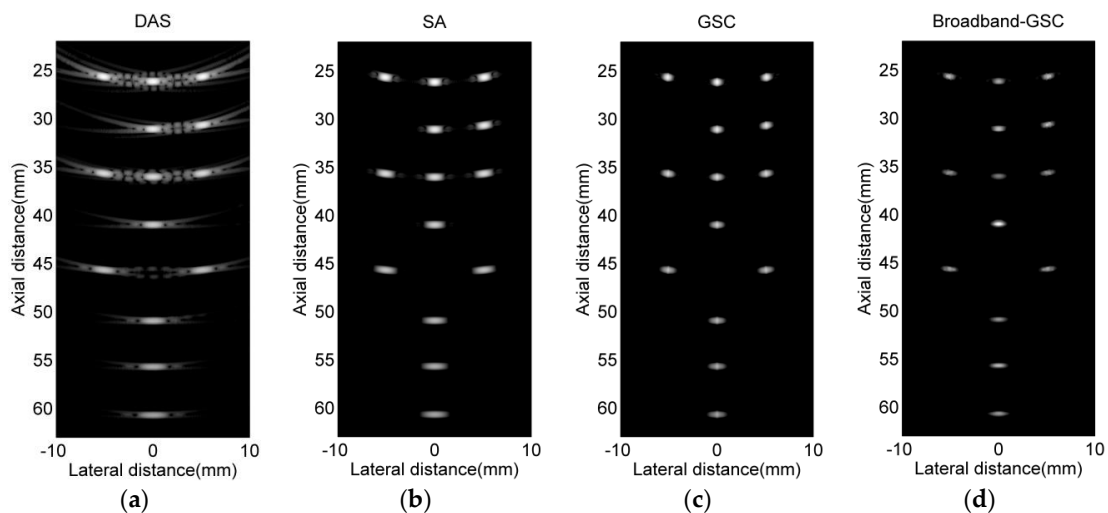


Figure 3. Beamforming responses of the 14 scattering point targets. (a) delay-and-sum (DAS); (b) synthetic aperture (SA); (c) generalized sidelobe canceler (GSC); (d) Broadband-GSC.

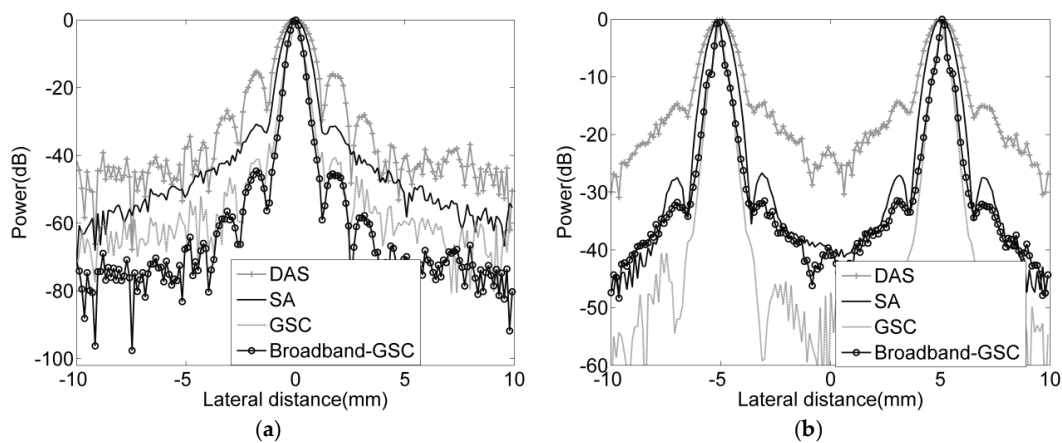


Figure 4. Lateral variation after each beamforming, (a) $z = 41$ mm; (b) $z = 45.8$ mm.

Taking depth $z = 41$ mm as reference, the PSL and FWHM after each beamforming are shown in Table 1. Broadband-GSC has almost the same FWHM as GSC, while the FWHM is increased by 43.2% and 58.0% compared with SA and DAS, respectively. The observation index PSL is used to indicate the inhibition of sidelobe energy. Broadband-GSC reduces the PSL by 11.6 dB and 26.4 dB compared with SA and DAS, respectively. Sidelobe energy represents the interference and noise signal, consequently, the lower PSL the better [25]. Beamforming responses indicate that Broadband-GSC can obviously improve the PSL and FWHM compared with DAS and SA.

Table 1. Full width at half maximum (FWHM) and peak sidelobe level (PSL) of the scattering point at depth $z = 41$ mm.

Beamforming	FWHM (mm)	PSL (dB)
DAS	1.50	−15.4
SA	1.11	−30.2
GSC	0.60	−41.8
Broadband-GSC	0.63	−44.6

Comparing GSC with Broadband-GSC, GSC needs both to receive and to transmit focused ultrasonic echo data. Therefore, all elements are ordinal excited and N 's receiving focused echo imaging has to be obtained. Broadband-GSC achieves an increase in lateral resolution and PSL with only one single emission, which reduces the system's hardware complexity. Consequently, Broadband-GSC reduces the beamforming process complexity, introduces the possibility for high frame-rate imaging with improved imaging quality.

4.2. Circular Cyst Experiments

Echo data for the circular cyst and scattering points in a high speckle noise environment are obtained. Several scattering points are set around the cyst, which have different and lower scattering coefficients to increase the background speckle noise [26,27]. Beamforming responses after different beamformings are shown in Figure 5. Figure 6 shows the lateral variation of the beamforming responses.

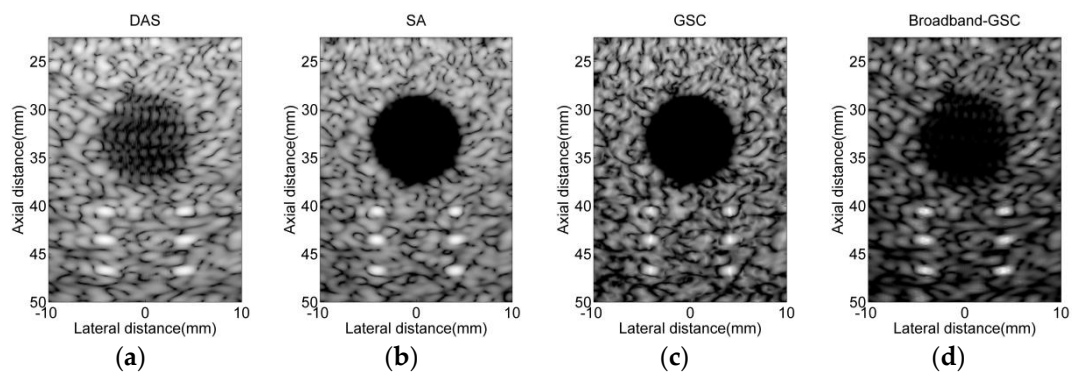


Figure 5. Simulated circular cyst and scattering points imaging in high speckle noise environment. (a) DAS; (b) SA; (c) GSC; (d) Broadband-GSC.

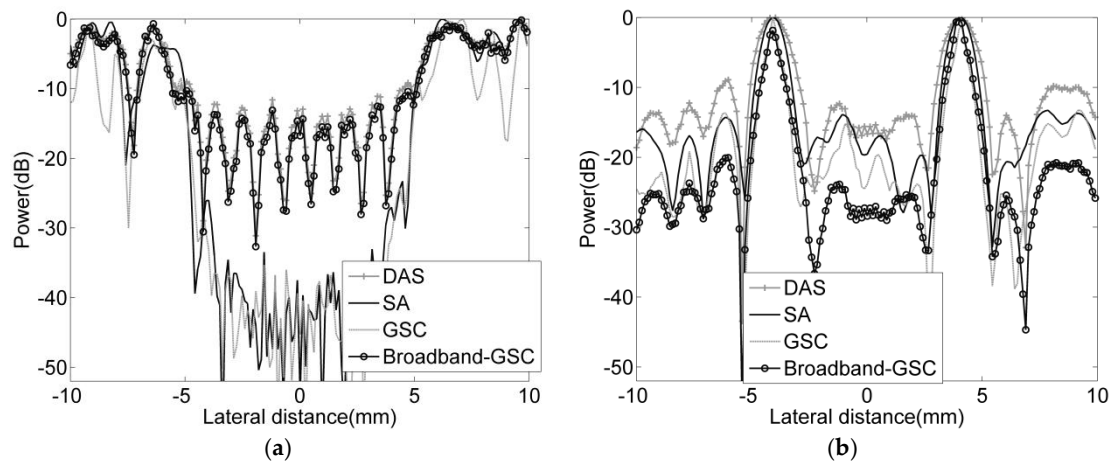


Figure 6. Lateral variation of each beamforming, (a) $z = 32$ mm; (b) $z = 46.7$ mm.

The lateral resolution of the scattering point at $(x, z) = (-4, 46.5)$ mm is 1.71, 1.29, 0.85 and 0.73 mm after DAS, SA, Broadband-GSC and GSC, respectively. Results show that the Broadband-GSC still can improve the lateral resolution compared with DAS and SA during the high speckle noise environment. Broadband-GSC improves the FWHM by 34.1% and 50.3% compared with SA and DAS, respectively. The results are the same as point targets experiments, which validate the effectiveness of the proposed beamforming.

Comparing the lateral variation after each beamforming at $z = 32$ mm, Broadband-GSC has almost the same result as DAS. Meanwhile, GSC generates the similar result as SA. The reason is that scatters do not have obviously higher signal-to-noise ratio (SNR) than background. The system's SNR also influences the performance of the adaptive beamforming. Reference [28] indicates that the performance of the adaptive beamforming is dependent on the system's SNR. When the system's SNR decreases, imaging quality after adaptive beamforming will rapidly decrease. Consequently, the advantages of combining plane wave emission with Broadband-GSC to improve both the system's SNR and lateral resolution will be discussed.

4.3. Plane Wave Emission Test

Plane wave emission is one of the most commonly used emission ways in commercial ultrasonic imaging products [29]. Commercial ultrasonic imaging systems need enough emission energy to achieve sufficient system signal-to-noise ratio (SNR). Therefore, the system will obtain better imaging quality with higher investigation depth [30]. Plane wave emission uses all elements to transmit and receive the ultrasonic; the entire imaging region will be covered with one single emission. Therefore, only DAS and Broadband-GSC can be introduced to process the echo signal after the plane wave emission. Beamforming responses of scattering points with plane wave emission are shown in Figure 7.

Beamforming responses indicate that the average FWHM of the scattering points are 1.38 mm and 0.77 mm after DAS and Broadband-GSC at $z = 40.6$ mm, respectively. Broadband-GSC improves the lateral resolution by 44.2% compared with DAS. Figure 8 also indicates that Broadband-GSC can reduce the sidelobe energy. Plane wave emission experiment indicates that Broadband-GSC can achieve an increase in lateral resolution with only one single emission. Consequently, Broadband-GSC will not only reduce the system's hardware complexity, but also introduce the possibility for higher investigation depth.

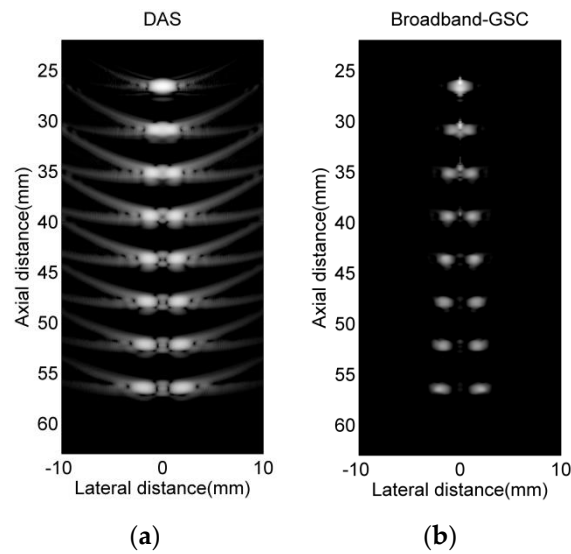


Figure 7. Beamforming responses of the 16 scattering point targets with plane wave emission. (a) DAS; (b) Broadband-GSC.

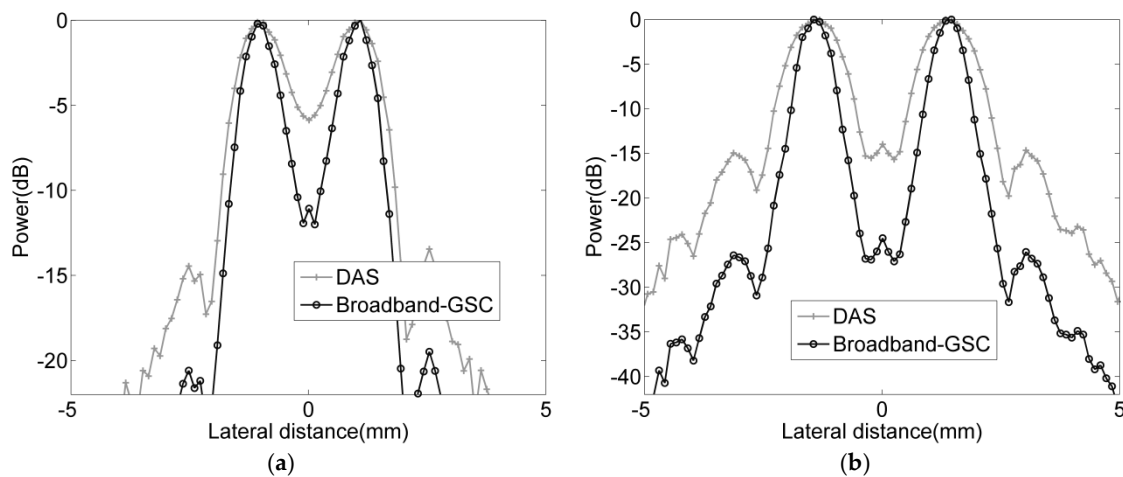


Figure 8. Lateral variation of each beamforming, (a) $z = 35.6$ mm; (b) $z = 40.6$ mm.

5. Discussion and Conclusions

The beamforming responses in Figure 3 are the key to understand the advantages of Broadband-GSC. Compared with traditional non-adaptive beamforming DAS and SA, Broadband-GSC will significantly improve the lateral resolution and restrain the interference and noise signal. Broadband-GSC only uses the receiving focused echo signal after DAS, which achieves an increase in lateral resolution with only one single emission. Compared with GSC, Broadband-GSC not only reduces the beamforming process complexity, but also reduces the system hardware complexity. Consequently, Broadband-GSC beamforming allows for high frame-rate imaging with increased imaging quality. The experiment of circular cyst shows that Broadband-GSC still can improve the lateral resolution and PSL even during the high speckle noise environment. Meanwhile, beamforming algorithms cannot improve the axial resolution. The axial resolution of the ultrasonic imaging system is determined by the center frequency of the ultrasonic f_0 , ultrasonic velocity c , and the emitted ultrasonic numbers. The axial resolution of system can be improved by algorithm like coded excitation.

Plane wave emission experiment changes the emission way of ultrasonic imaging system. Plane wave emission will use all elements to transmit ultrasonic, therefore, improves the system’s SNR to obtain higher investigation depth. The system’s SNR also influences the performance of the

adaptive beamforming. Previous work [28] indicates that the performance of adaptive beamforming is dependent on the system's SNR. When system's SNR decreases, imaging quality after adaptive beamforming will rapidly decrease. Hence, plane wave emission still is one of the most commonly used emission methods in commercial ultrasonic imaging products. Results indicate that Broadband-GSC can achieve an increase in lateral resolution and PSL with only one single emission. Therefore, Broadband-GSC can be introduced to deal with the received echo data after plane wave emission.

Broadband-GSC introduces the discrete wavelet transform to divide the broadband echo signal into a set of narrowband signals. Therefore, narrowband methods can be applied directly on broadband ultrasonic data. Basing on adaptive beamforming GSC, a set of adapted, data-dependent apodization weights for each wavelet subband are provided. Broadband-GSC can both maintain the desired signal and suppress the interference and noise signal, therefore, improves the system imaging quality. Furthermore, Broadband-GSC achieves an increase in lateral resolution with only one single emission. New beamforming reduces the algorithm process complexity and the system's hardware complexity. Broadband-GSC introduces the possibility for higher frame-rate and higher investigation depth with better imaging quality.

Author Contributions: Conceptualization, J.L. and X.C.; Methodology, L.M. and Z.M.; Software, H.C., Y.W. and Z.W.; Validation, J.L., L.M. and Z.M.; Formal Analysis, J.L., L.M. and Z.W.; Investigation, J.L. and Z.M.; Resources, J.L.; Data Curation, J.L. and Z.W.; Writing—Original Draft Preparation, J.L., L.M. and Z.M.; Writing—Review & Editing, J.L., H.C. and Y.W.; Visualization, L.M. and Z.M.; Supervision, X.C. and Z.M.; Project Administration, L.M. and Z.M.; Funding Acquisition, H.C., Y.W. and X.C. All authors have read and agreed to the published version of the manuscript.

Funding: This research was funded by [China National Key R&D Program during the 13th Five-year Plan Period] grant number [2018YFC0116200] and [China National Key R&D Program during the 13th Five-year Plan Period] grant number [2017YFC0109702].

Conflicts of Interest: The authors declare no conflict of interest.

References

1. Synnevag, J.F.; Austeng, A.; Holm, S. Benefits of minimum-variance beamforming in medical ultrasound imaging. *IEEE Trans. Ultrason. Ferroelectr. Freq. Control* **2009**, *56*, 1868–1879. [[CrossRef](#)] [[PubMed](#)]
2. Bottenus, N.; Byram, B.C.; Dahl, J.J.; Trahey, G.E. Synthetic aperture focusing for short-Lag spatial coherence imaging. *IEEE Trans. Ultrason. Ferroelectr. Freq. Control* **2013**, *60*, 1816–1826. [[CrossRef](#)] [[PubMed](#)]
3. Guo, W.; Wang, Y.; Yu, J. Ultrasound harmonic enhanced imaging using eigenspace-based coherence factor. *Ultrasonics* **2016**, *72*, 106–116. [[CrossRef](#)] [[PubMed](#)]
4. Li, J.; Chen, X.; Wang, Y.; Chen, X.; Yu, D. Forward-backward generalized sidelobe canceler beamforming applied to medical ultrasound imaging. *AIP Adv.* **2017**, *7*, 015201. [[CrossRef](#)]
5. Sakhaei, S.M. A decimated minimum variance beamformer applied to ultrasound imaging. *Ultrasonics* **2015**, *59*, 119–127. [[CrossRef](#)] [[PubMed](#)]
6. Hyun, D.; Abou-Elkacem, L.; Perez, V.A.; Chowdhury, S.M.; Willmann, J.K.; Dahl, J.J. Improved sensitivity in ultrasound molecular imaging with coherence-based beamforming. *IEEE Trans. Med. Imaging* **2018**, *37*, 241–250. [[CrossRef](#)]
7. Li, J.; Chen, X.; Wang, Y.; Li, W.; Yu, D. Eigenspace-based generalized sidelobe canceler beamforming applied to medical ultrasound imaging. *Sensors* **2016**, *16*, 1192. [[CrossRef](#)]
8. Sakhaei, S.M.; Shamsian, S.E. Twofold minimum variance beamforming for enhanced ultrasound imaging. *J. Med. Ultrason.* **2018**, *45*, 17–24. [[CrossRef](#)]
9. Chau, G.; Dahl, J.; Lavarello, R. Effects of phase aberration and phase aberration correction on the minimum variance beamformer. *Ultrason. Imaging* **2018**, *40*, 15–34. [[CrossRef](#)]
10. Holfort, I.K.; Gran, F.; Jensen, J.A. Minimum variance beamforming for high frame-rate ultrasound imaging. In Proceedings of the 2007 IEEE International Ultrasonics Symposium, New York, NY, USA, 28–31 October 2007; pp. 1541–1544.
11. Holfort, I.K.; Gran, F.; Jensen, J.A. Broadband minimum variance beamforming for ultrasound imaging. *IEEE Trans. Ultrason. Ferroelectr. Freq. Control* **2009**, *56*, 314–325. [[CrossRef](#)]

12. Nicolae, I.D.; Marinescu, R.F.; Nicolae, P.M.; Cristina, M.D. Limits and usability of fast Fourier, discrete wavelet and wavelet packet transforms applied at signals from a primary winding of a locomotive transformer. In Proceedings of the 2017 International Conference on Electromechanical and Power Systems (SIELMEN), Iasi, Romania, 11–13 October 2017; pp. 462–467.
13. Pei, S.C.; Hsue, W.L. The multiple-parameter discrete fractional fourier transform. *IEEE Signal Process. Lett.* **2006**, *13*, 329–332.
14. Liu, D.; Schaible, K.; Low, W.; Ebbini, E.S. Three-dimensional image guidance for transcranial focused ultrasound therapy. In Proceedings of the IEEE 14th International Symposium on Biomedical Imaging (ISBI 2017), Melbourne, Australia, 18–21 April 2017; pp. 916–919.
15. Kortbek, J.; Jensen, J.A.; Gammelmark, K.L. Sequential beamforming for synthetic aperture imaging. *Ultrasonics* **2013**, *53*, 1–16. [[CrossRef](#)]
16. Jensen, J.A.; Nikolov, S.I.; Gammelmark, K.L.; Pedersen, M.H. Synthetic aperture ultrasound imaging. *Ultrasonics* **2006**, *44*, 5–15. [[CrossRef](#)] [[PubMed](#)]
17. Li, J.; Chen, X.; Wang, Y.; Yu, D. Sidelobe Canceller Algorithm for Ultrasonic Imaging. *Laser Optoelectron. Prog.* **2019**, *56*, 071103.
18. Li, J.; Chen, X.; Wang, Y.; Shi, Y.; Yu, D. Generalized sidelobe canceler beamforming applied to medical ultrasound imaging. *Acoust. Phys.* **2017**, *63*, 229–236. [[CrossRef](#)]
19. Albulayli, M.; Rakhmatov, D. Hybrid adaptive/nonadaptive beamforming for ultrasound imaging. In Proceedings of the 2013 IEEE International Conference on Acoustics, Vancouver, BC, Canada, 26–31 May 2013; pp. 1061–1065.
20. Shan, T.-J.; Kailath, T. Adaptive beamforming for coherent signals and interference. *IEEE Trans. Acoust. Speech. Signal Process.* **1985**, *33*, 527–536. [[CrossRef](#)]
21. Wang, Z.; Li, J.; Wu, R. Time-delay- and time-reversal-based robust capon beamformers for ultrasound imaging. *IEEE Trans. Med. Imaging* **2005**, *24*, 1308–1322. [[CrossRef](#)]
22. Jensen, J.A.; Svendsen, N.B. Calculation of pressure fields from arbitrarily shaped, apodized, and excited ultrasound transducers. *IEEE Trans. Ultrason. Ferroelec. Freq. Control* **1992**, *39*, 262–267. [[CrossRef](#)]
23. Jensen, J.A. Field: A program for simulating ultrasound systems. *Med. Biol. Eng. Comput.* **1996**, *34*, 351–353.
24. Zeng, X.; Wang, Y. Beam-domain eigenspace-based minimum variance beamformer for medical ultrasound imaging. *IEEE Trans. Ultrason. Ferroelectr. Freq. Control* **2013**, *60*, 2670–2676. [[CrossRef](#)]
25. Nilsen, C.I.; Hafizovic, I. Beamspace adaptive beamforming for ultrasound imaging. *IEEE Trans. Ultrason. Ferroelec. Freq. Control* **2009**, *56*, 2187–2197. [[CrossRef](#)] [[PubMed](#)]
26. Li, J.; Stoica, P.; Wang, Z. Doubly constrained robust capon beamformer. *IEEE Trans. Signal Process.* **2004**, *52*, 2407–2423. [[CrossRef](#)]
27. Rombouts, G.; Spriet, A.; Moonen, M. sidelobe canceller based combined acoustic feedback- and noise cancellation. *Signal Process.* **2008**, *88*, 571–581. [[CrossRef](#)]
28. Synnevag, J.F.; Austeng, A.; Holm, S. Adaptive beamforming applied to medical ultrasound imaging. *IEEE Trans. Ultrason. Ferroelec. Freq. Control* **2007**, *54*, 1606–1613. [[CrossRef](#)]
29. Wang, Y.; Zheng, C.; Peng, H.; Chen, X. Short-lag spatial coherence combined with eigenspace-based minimum variance beamformer for synthetic aperture ultrasound imaging. *Comput. Biol. Med.* **2017**, *91*, 267–276. [[CrossRef](#)]
30. Zhao, J.; Wang, Y.; Yu, J.; Guo, W.; Li, T.; Zheng, Y.P. Subarray coherence based postfilter for eigenspace based minimum variance beamformer in ultrasound plane-wave imaging. *Ultrasonics* **2016**, *65*, 23–33. [[CrossRef](#)]

